Hindawi Publishing Corporation
Conference Papers in Science
Volume 2015, Article ID 276374, 10 pages
http://dx.doi.org/10.1155/2015/276374

Conference Paper

Effect of Dilution on Microstructure and Wear Resistance of a Fe-Based Hardfacing Alloy with a High Amount of Carbide-Forming Elements

L. Rovatti,[1] J. N. Lemke,[1] N. Lecis,[1] O. Stejskal,[2] and M. Vedani[1]

[1] *Dipartimento di Meccanica, Politecnico di Milano, Milan, Italy*
[2] *Bernex Bimetallic S.r.o., Modrice Bei Brno, Czech Republic*

Correspondence should be addressed to L. Rovatti; ludovica.rovatti@polimi.it

Received 1 August 2014; Revised 23 September 2014; Accepted 7 October 2014

Academic Editor: Martin Dienwiebel

This Conference Paper is based on a presentation given by M. Vedani at "European Symposium on Friction, Wear, and Wear Protection" held from 6 May 2014 to 8 May 2014 in Karlsruhe, Germany.

Hardfacing is a widely diffused technique adopted to increase service life of parts for heavy-duty applications. Even though hardfacing alloys feature optimized chemistry and microstructure for specific service conditions, dilution with substrate modifies the resulting properties along a significant fraction of the deposit thickness. In particular, C and B diffusion to the substrate alters hypereutectic alloys reducing the carbide-forming ability and modifying the solidification sequence. In the present paper, the effect of dilution on a hypereutectic Fe-C-B based alloy containing Cr and Mo was investigated. The effect of dilution on the reference alloy was studied by producing laboratory castings with an increased amount of Fe, up to 50 mass %. The obtained results were compared with the dilution of the hardfacing alloy cast on steel substrates. The microstructural evolution was analyzed by XRD (X-ray diffraction), differential scanning calorimetry (DSC), optical microscopy (OM), and scanning electron microscopy (SEM), whereas mechanical behaviour was evaluated by hardness measurements and wear resistance by pin-on-disc tests.

1. Introduction

White cast iron is known for its excellent resistance to abrasion and oxidation and has been widely used in aggressive conditions, including mining and mineral processing, cement industry, and polymer extrusion [1–3]. Alloys containing a high amount of carbide-forming elements can be utilized not only like as-cast products, but also like hardfacing alloys for producing deposits with thickness up to the millimeter scale. Low-carbon Fe-based hardfacing alloys are usually selected for situations involving moderate abrasion and impact loads, whereas the higher-carbon hypereutectic alloys are used for applications featuring severe abrasion and limited impact applications due to their lower fracture toughness [2, 4, 5]. Suitable deposition processes of hardfacing alloys rely on welding-based techniques (e.g., tungsten inert gas deposition and plasma transferred arc), on laser cladding, or on spin casting of the molten alloy inside hollow parts [6]. Nowadays, controlling dilution is gaining importance for all the abovementioned deposition techniques, in order to obtain high quality coatings [6, 7]. In literature geometric and chemical dilutions are defined [7]. The geometric dilution is a function of deposit height and depth, while the chemical dilution is related to the enrichment of element diffusing from the substrate toward the deposit [7]. Particularly in the case of hardfacing alloys containing a high amount of alloying elements, controlling chemical dilution represents a key factor for realizing coatings with high tribological properties throughout their volume. In fact, if a minimum dilution is necessary to guarantee a good metallurgical bonding between coating and substrate, an excessive dilution does not allow preservation of the optimized chemical composition and homogeneous properties of the coating. The dilution depends on the diffusion of the elements from and toward

Table 1: Composition (mass %) of the base alloy and diluted alloys.

	C + B	Ni	Mn	Cr	Si	V	Mo	Cu	Fe
Base alloy	5.72	4.46	0.50	9.7	2.04	0.09	5.29	1.20	Bal.
Base alloy + 20Fe	4.59	3.20	0.22	7.61	1.66	0.08	4.30	1.19	Bal.
Base alloy + 30Fe	4.02	2.80	0.19	6.66	1.46	0.07	3.76	1.04	Bal.
Base alloy + 40Fe	3.44	2.40	0.16	5.71	1.25	0.06	3.22	0.89	Bal.
Base alloy + 50Fe	2.87	2.00	0.14	4.76	1.04	0.05	2.69	0.75	Bal.

the substrate and on the melting of a small area of the substrate during the deposition. Hence, according to the Arrhenius equation, temperature, alloy composition, and cooling rate are process parameters to be evaluated [8, 9]. In particular, the diffusion of the interstitial elements, like C and B, could widely modify the solidification range of the alloy with a significant effect on the formation of porosities during the deposition process. It is established that the wider the solidification range, the higher the hot cracking probability in cast alloys [10]. There are a few studies carried out with a systematic approach on the effects of chemical dilution on the microstructure, melting behavior, hardness, and wear resistance of hardfacing alloys deposited by welding techniques [11, 12].

In this research, possible detrimental effects of the chemical dilution have been analyzed. In a first step the dilution of the base alloy was simulated by a gradual addition of pure Fe. In a second step, more representative dilution conditions were generated by casting the hardfacing alloy directly in a steel crucible. The proposed approach was specifically developed to simulate the spin casting process used to produce hard inlay layers on the inner surface of large barrels to be used, for instance, in polymer extrusion industry. This process has to be considered as a sort of centrifugal casting where a low-melting point alloy is spun against the inner surface of a pipe, inducing important effects related to dilution of the hardfacing alloy with the substrate.

2. Materials and Experimental Procedures

In a first stage, the addition of the pure Fe powders to the base alloy was selected in order to simulate different dilution levels starting from 20% up to 50% (in mass %), obtaining the compositions reported in Table 1.

After blending, the powders were placed in alumina crucibles and melted. In the second stage, casting of the hardfacing alloy directly in steel crucibles was realized using molds with a size of 30 mm in length, 15 mm in width, and 10 mm in depth (see Figure 1). The thermal cycle applied for the melting was similar to that currently used in industrial processing in a furnace equipped with a flow of Ar as shielding gas. DSC was used to measure liquidus and solidus temperatures as well as solid-state phase transformations of the alloys. DSC thermograms were generated by imposing a heating ramp up to 1250°C at a rate of 30°C/min and 15-minute holding at maximum temperature followed by a cooling step at the same rate on samples of about 100 mg, in an argon gas atmosphere. In particular, heat flow was recorded as a function of temperature and by analyzing the cooling curves the offset and onset points of the melting and solidification ranges were determined.

X-ray diffraction (XRD) analyses were performed to identify alloy phases found after solidification of the powders. XRD measurements were carried out by a PANalytical X-Pert PRO instrument, with a θ-θ configuration, equipped with a RTMS X'Celerator sensor. CuKα ($\lambda = 0,15418$ nm) radiation was employed to perform the tests. The XRD spectra were evaluated using the JCPDS database. Microstructural investigations were carried out after metallographic polishing and etching with Nital 2% and Marble solution, using an optical microscope (OM) by Leitz Aristomet and a scanning electron microscope (SEM) by Zeiss EVO 50, generally operated at an accelerating tension of 20 KeV with a working distance of 10 mm in secondary electron (SE) and backscattered electron (BSE) mode. The "ImageJ" software was adopted for measuring the phase volume fraction. Macrohardness tests were carried out using Vickers equipment with a load of 294.3 N on the indenter, while microhardness was performed with a load of 19.6 N to realize hardness profiles in the welded microstructure. Wear tests were carried out on sectioned samples using a pin-on-disc tribometer by CSM Instruments with a Si_3N_4 ball (diameter of 6 mm) as a pin, at linear sliding speed of 0.1 m/s along a circular path of about 10 mm in diameter. A normal load of 5 N was used for about 9000 cycles, corresponding to a sliding distance of 300 m. Wear tracks were observed by SEM and their profiles were measured using a contact profilometer from which the volume loss was determined once the wear track length was known.

3. Results and Discussion

3.1. Solidification Behavior and Microstructure after Dilution. The reference alloy is made of Cr-rich carbides and borides, with a volume fraction of 84 ± 4.65%, of a metallic phase, and of Mo-rich phases characterized by two different morphologies: lamellar and blocky shapes. The different phases detected in the base alloy are described in the OM and in SEM micrographs of Figure 2 as well as in the XRD spectrum of Figure 3.

In particular EDS and XRD analysis revealed the presence of M_2B borides, with a tetragonal crystal structure, M_7C_3 carbides (D, C point analysis of Figure 2), $M_{23}(C, B)_6$, $M_3(C, B)$ carboborides (B point analysis of Figure 2), and α-Fe matrix. These results are consistent with the microstructure observed by Röttger et al. in a FeCrMoCB hardfacing alloy (X200CrNiBMo10-4-3-3 steel) with a chemical composition very close to the base alloy studied in this research [13].

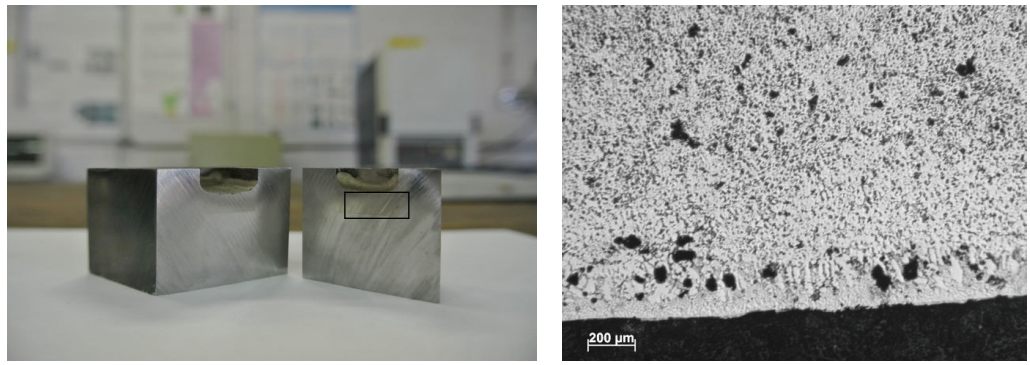

(a) (b)

Figure 1: Cross-section of the steel crucible after melting of the hardfacing alloy (a). (b) A magnification of the interface between the coating and the substrate.

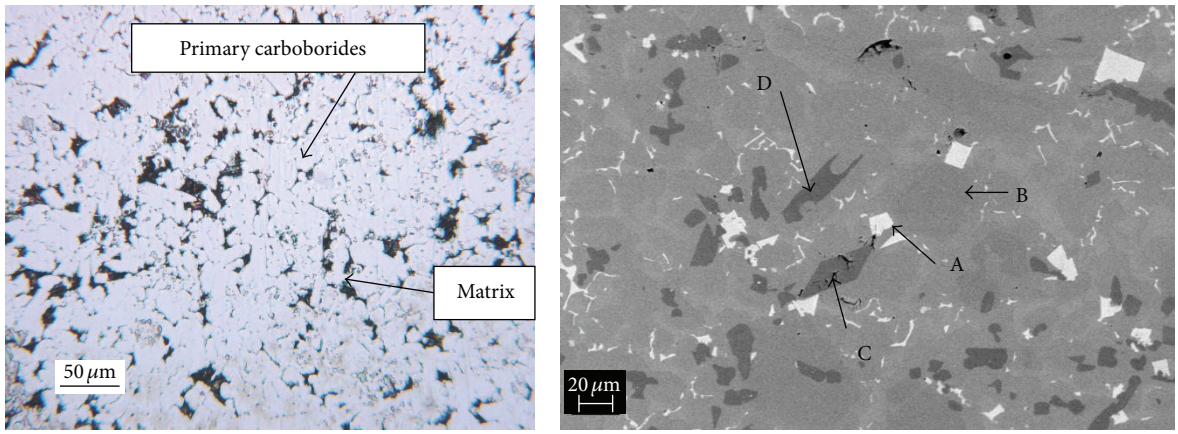

(a) (b)

Point analysis	Si	V	Cr	Mn	Ni	Cu	Mo	Fe
A	0.03	0.36	9.06	0	0.63	0.07	63.23	Bal.
B	0.12	0.31	21.13	0.16	1.67	0.34	7.4	Bal.
C	0.04	0.05	15.63	0.39	1.8	0.15	2.22	Bal.
D	0	0	17.10	0.19	2.03	0.22	2.58	Bal.

(c)

Figure 2: Microstructure of the reference alloy: OM (a) and SEM-BSE micrograph (b). The table contains the EDS microanalysis related to the point analysis of (b).

The primary M_2B and M_7C_3 phases appear as darker phases in BSE images. On the contrary, Mo-rich phases appear as brighter phases owing to the high content of heavier elements (A point analysis of Figure 2). Considering the low amount of the Mo-rich phases, as it will be discussed below, it was difficult to establish the crystallography of these phases through XRD analysis. However, as reported by Röttger et al., the Mo-rich M_3B_2 borides were detected in these FeCrMoCB hardfacing alloys [13].

The microstructure of the diluted alloys after the different Fe additions is reported in Figure 4 (OM micrographs) and in Figure 5 (SEM-BSE micrographs).

It is revealed that the diluted alloys featured a hypereutectic solidification mode, up to high dilution rates of 30%: at this level the microstructure became near-eutectic (Figure 4(b)) and at 40% and 50% dilution primary metallic dendrites with a bainitic-martensitic structure were observed (see Figures 4(c), 4(d) and 5(c), 5(d)). Moreover, for Fe level exceeding 30%, the presence of the M_2B borides and M_7C_3 Cr-rich carbides was suppressed and the presence of a high amount of eutectic structure was detected (see Figures 4(c) and 5(c)).

The volume fractions of the primary phases and of M_2B, M_7C_3, and Mo-rich phases as a function of dilution levels are reported in Figure 6. As already mentioned, the eutectic

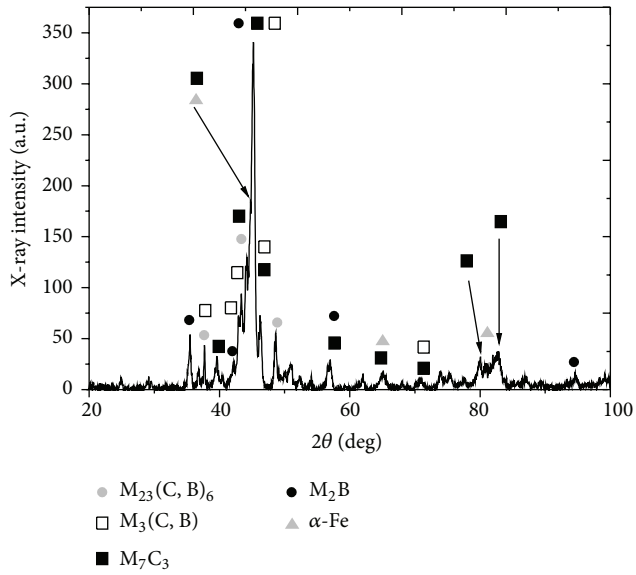

Figure 3: XRD spectra of the investigated hardfacing alloy.

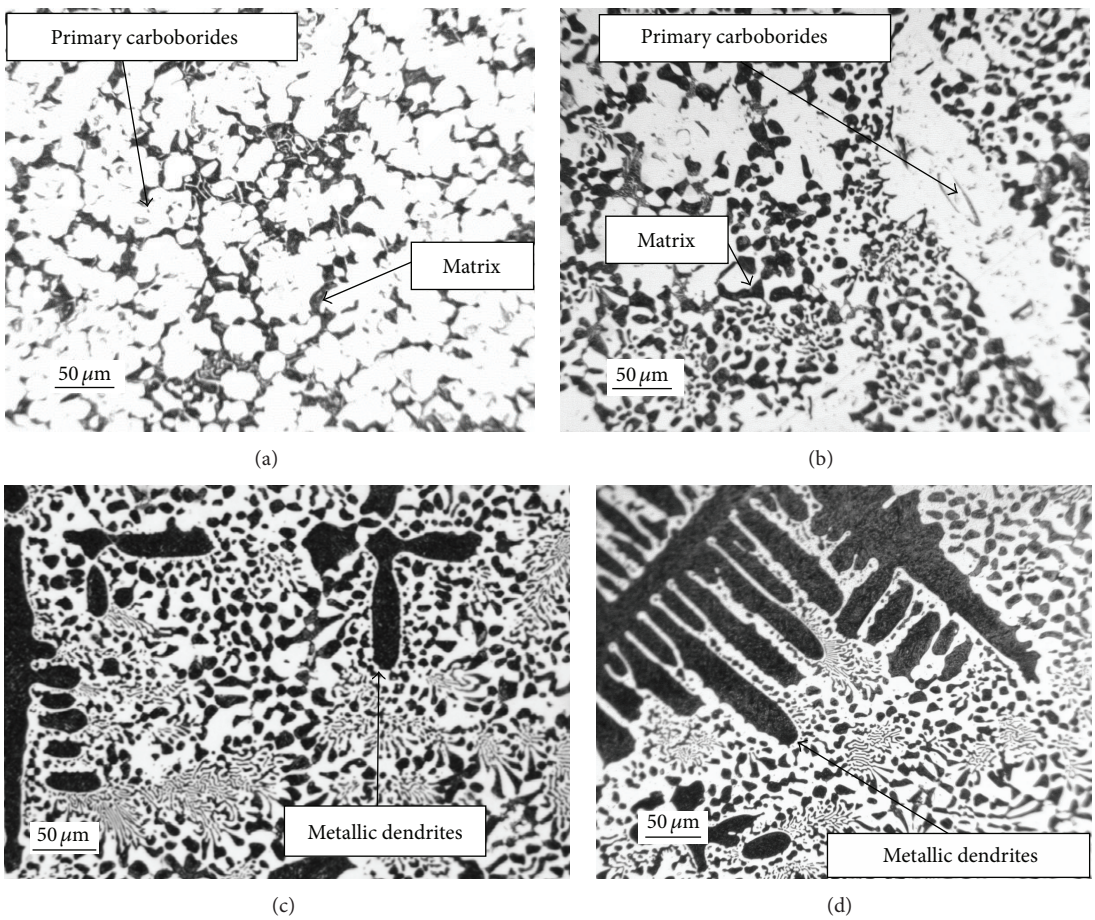

Figure 4: Optical micrographs of the diluted alloys with different Fe addition: 20 mass % Fe (a), 30 mass % Fe (b), 40 mass % Fe (c), and 50 mass % Fe (d).

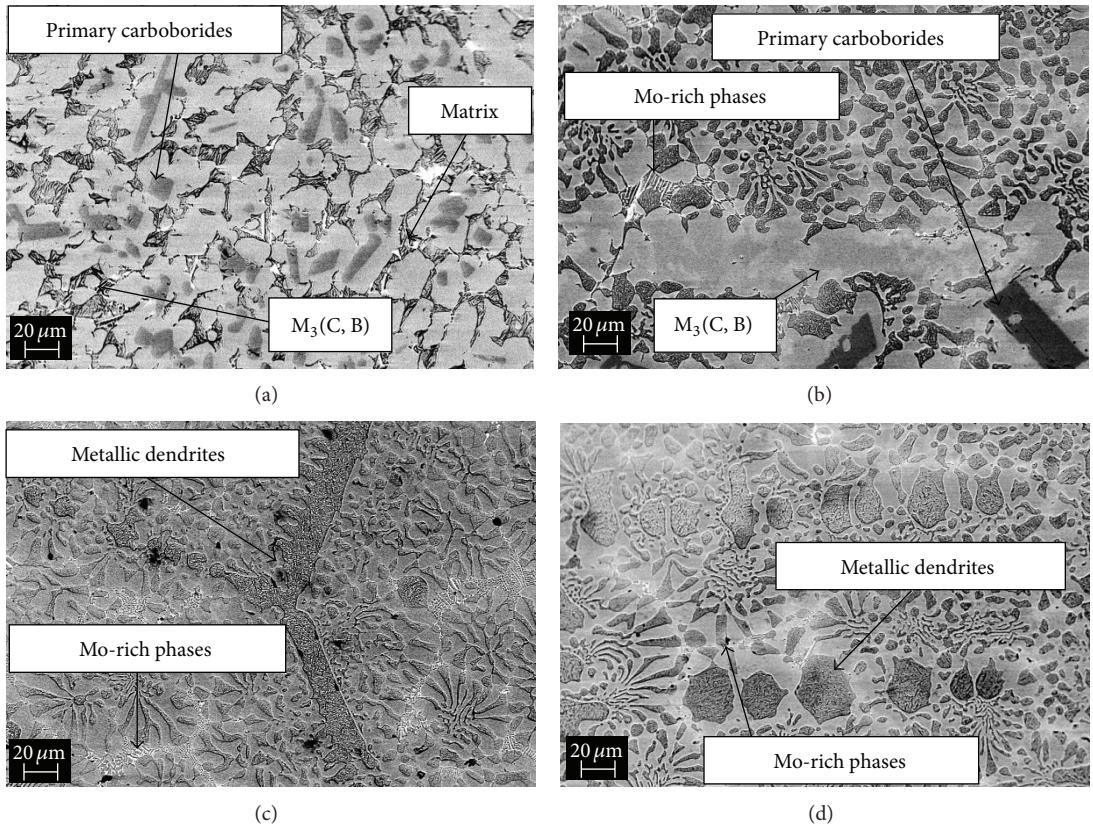

Figure 5: SEM-BSE micrographs of the diluted alloys: 20 mass % Fe (a), 30 mass % Fe (b), 40 mass % Fe (c), and 50 mass % Fe (d).

composition corresponds to a dilution rate close to 30% Fe (Figure 6(a)).

The lamellar Mo-rich phase content decreased with increasing dilution rate and remained almost constant at the highest levels of dilution. The blocky Mo-rich phase, on the contrary, decreased down to zero at the maximum dilution rates (Figure 6(b)).

The effect of the dilution on the solidification interval of the diluted alloys is depicted in Figure 7. By increasing the dilution, the solidification temperatures were shifted to higher values but the solidification range remained almost constant at a value of 87 ± 7°C up to 30% dilution. In correspondence to this Fe addition, the solidification gap reached a minimum value. This result is consistent with the near-eutectic microstructure of the alloy where the low melting eutectic solidifies.

After the eutectic point, the gap increased again for the highest dilution levels obtaining a solidification range close to that measured for the pure alloy. As it is known too small solidification ranges could be detrimental for the hardfacing alloy deposition process due to the difficulty for the liquid alloy to fill the interdendritic voids during solidification. On the contrary, too wide solidification range alloys were revealed to be much more prone to hot cracking [10].

3.2. Hardness and Wear Behavior. In order to analyze the hardness behavior of the base alloy after dilution, the macrohardness of the alloys with the increasing Fe levels (Figure 8) was measured. Hardness remained substantially unchanged by the first addition of 20% Fe (original alloy hardness was 911 ± 32.12, and 20% diluted alloy hardness became 923 ± 7.78), whereas, above 20% Fe dilution, it markedly decreased due to the reduced fraction of primary hard phases and of Mo-rich blocky phases and due to the shift to the hypoeutectic microstructure (see Figures 3 and 4).

For analyzing the possible effects of the dilution on wear properties, the nondiluted alloy and the diluted alloy with 30% of Fe addition were compared by pin-on-disc tests. This value of Fe addition was selected in order to reproduce a real microstructure of the base alloy obtained after the deposition in a region close to the steel substrate.

The evolution of the friction coefficient of the base alloy and of the diluted alloy is shown in Figure 9, while the volume loss data are reported in Table 2.

A volume loss three times lower was measured in the original base alloy when compared to the diluted alloy.

In the worn surface of the original hardfacing alloy were detected only shallow grooves as shown in Figure 11(a). This result is in accordance with the high hardness of the alloy itself (Figure 8). On the contrary, in the diluted alloy the wear grooves appeared deeper and with a larger number of sharp scratches as an evidence of the ploughing action generated by the worn debris on the relatively softer alloy surface. Moreover, the surface oxidation effect was more evident in the diluted alloy, as confirmed by the BSE micrographs of the

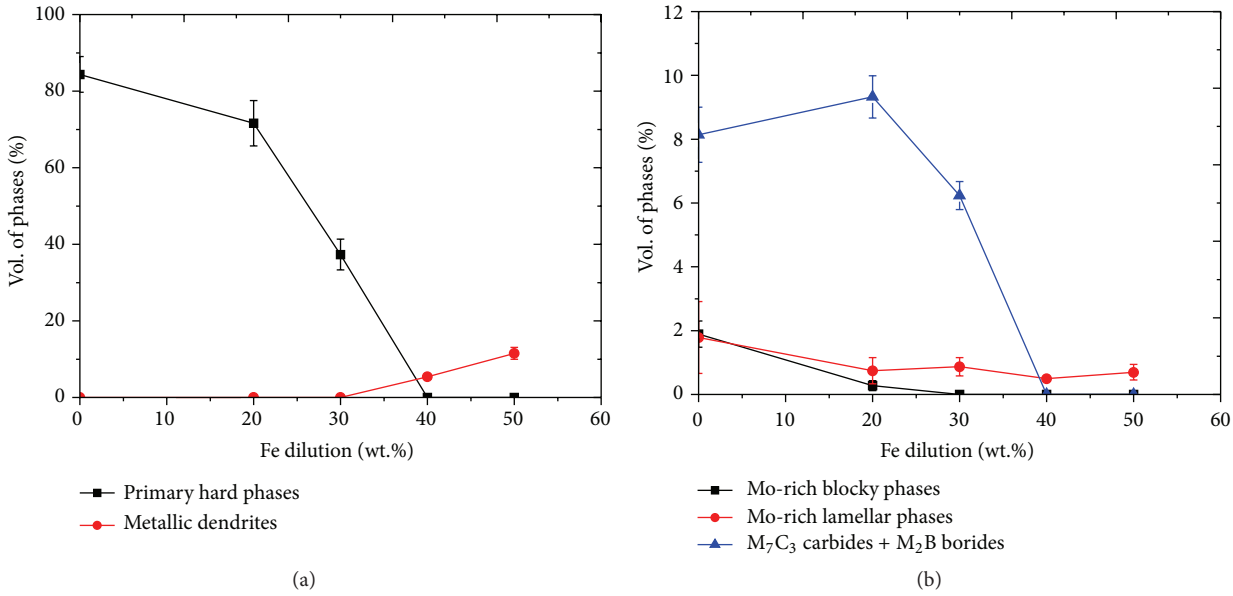

FIGURE 6: Primary phase evolution with increasing dilution rate (a), fraction of the M_7C_3 carbides, M_2B borides, and Mo-rich phases in the diluted alloys (b).

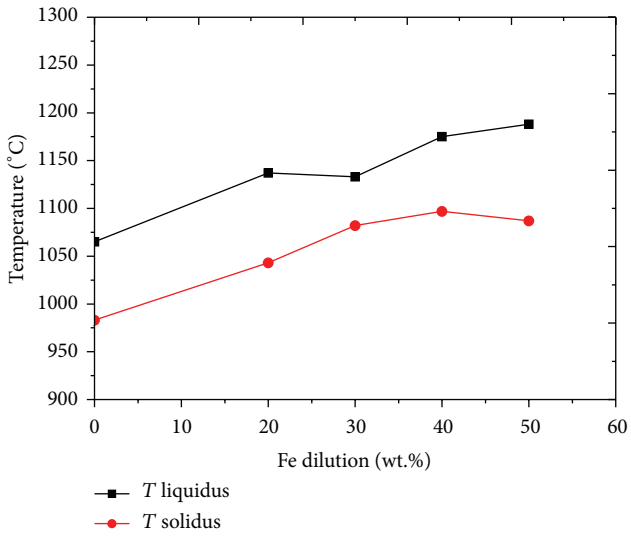

FIGURE 7: Solidification ranges of the base alloy and of the diluted alloys.

TABLE 2: Volume loss of the investigated alloys after wear tests.

Alloy	Volume loss (μm^3)
Base alloy	$384 \times 10^4 \pm 44.7$
Base alloy + 30Fe	$1193 \times 10^4 \pm 70.3$

tracks and by EDS microanalysis (Figure 10), probably related to the lower amount of hard phases (see Figure 6(a)).

3.3. Microstructural Evolution of the Base Alloy after Melting in the Steel Crucible. In Figure 11 the microstructural evolution

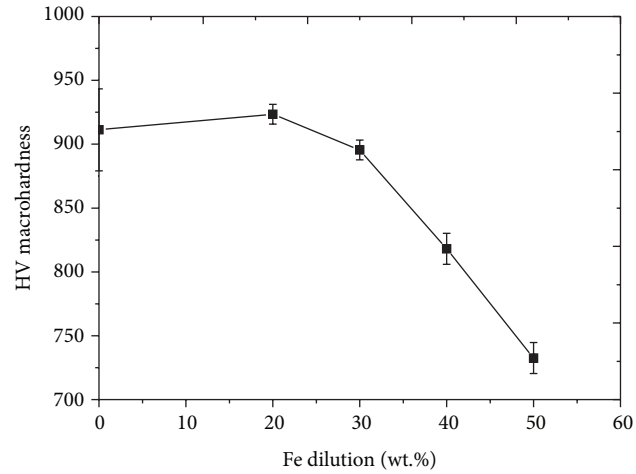

FIGURE 8: Macrohardness of the base alloy and of the diluted alloys.

along the thickness of the hardfacing alloy is shown after melting and solidification in the steel crucible.

The middle and the top parts of the coating alloy show an evident hypereutectic microstructure close to that observed in the original alloy (see Figure 2). On the contrary, close to the interface between the hardfacing alloy and the substrate, a 300 μm layer characterized by an eutectic structure was detected. Considering the microstructural evolution of the diluted alloys (Figures 4 and 5), this area has a near-eutectic microstructure that corresponds to a dilution level higher than 30%, with the presence of Mo-rich lamellar phases and without M_2B and M_7C_3 phases (see Figure 11(f)). Moreover, local melting of the substrate occurs during the process as can be observed by the irregularities at the interface between the coating and the substrate (Figure 11(f)).

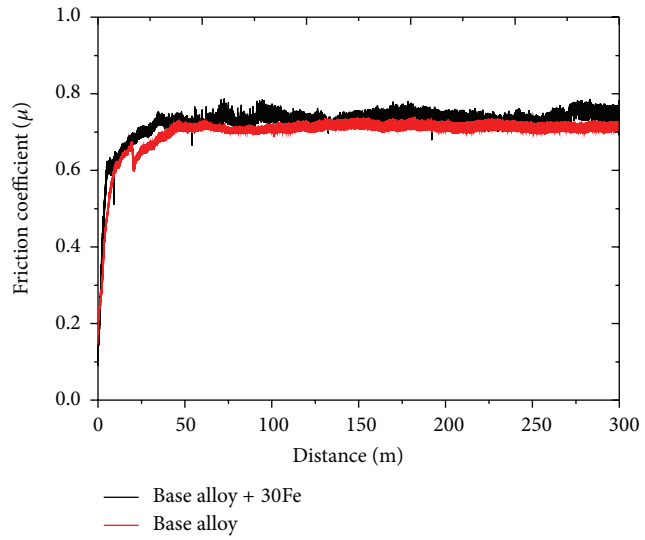

FIGURE 9: Evolution of the friction coefficient of base alloy and diluted alloy.

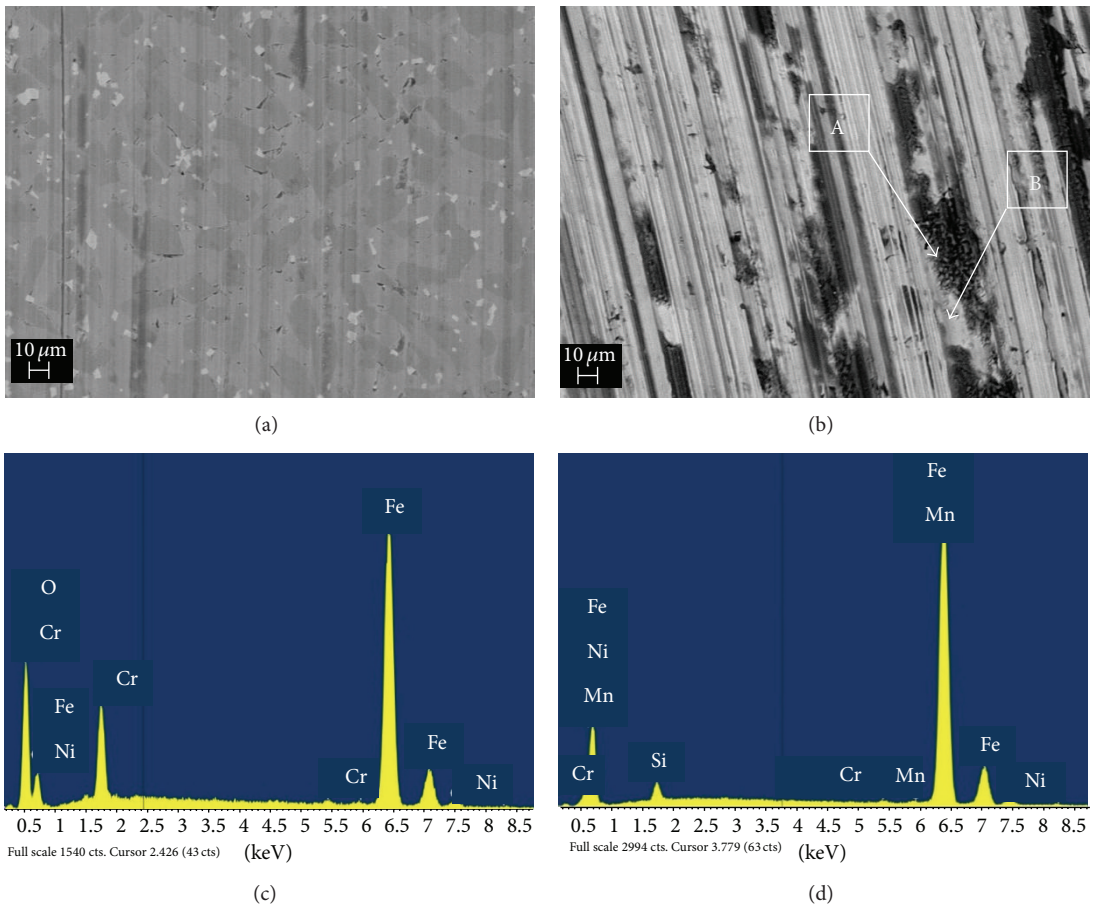

FIGURE 10: SEM micrographs obtained by SEM-BSE of the wear tracks of the base alloy (a) and of the diluted alloy with 30% of Fe (b), tested after a sliding distance of 300 m. The reported spectra (c) and (d) are, respectively, related to the points A and B of (b).

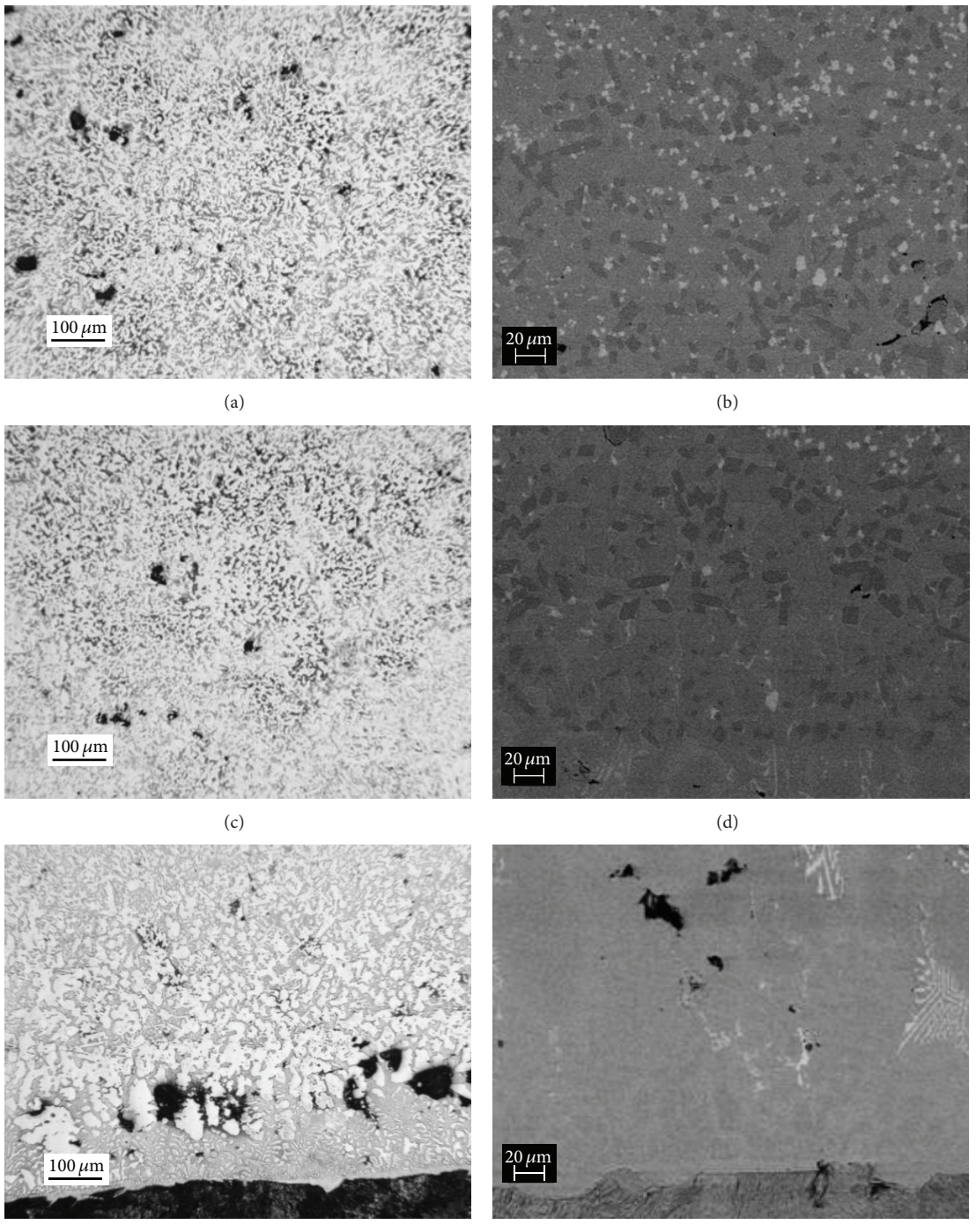

Figure 11: Optical and SEM-BSE micrographs of the hardfacing alloy melted in the steel crucible taken at different positions on cross-sectioned samples: top (a), (b), middle (c), (d), and bottom part (close to interface with the substrate) (e), (f).

Several porosities were detected in the region where the most evident microstructural changes have been detected, moving from the eutectic to the hypereutectic structure. One possible reason of this phenomenon can be the difference in the solidification ranges between the high diluted alloy at the interface and the hypereutectic alloy of the remaining volume of the coating. As it was observed by the DSC measurements, the solidification range of the diluted alloys reached a minimum value in correspondence to the eutectic composition with the increasing of solidification temperature (Figure 7). The hardness profile measured along the cross-section of the alloy cast in the steel crucible is reported in Figure 12. The

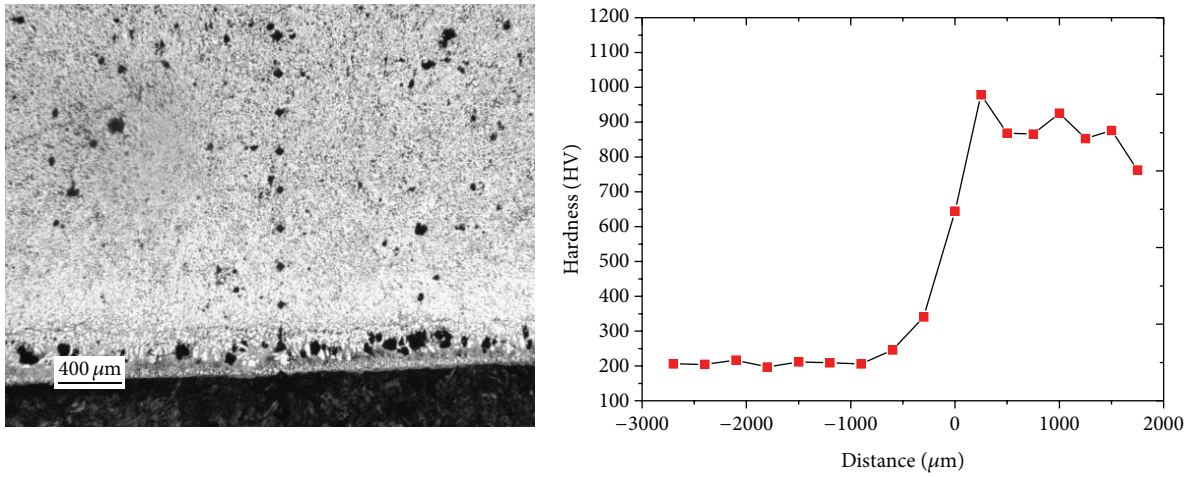

Figure 12: Cross-section (a) and corresponding hardness profile of the base alloy cast in the steel crucible (b).

obtained results are consistent with the previous hardness measurements and with the microstructural results showed above (see Figures 8 and 11).

At the interface with the substrate, a lower hardness value was measured in correspondence to the eutectic structure. On the contrary, the middle and the top regions were characterized by hardness values close to that measured in the original hardfacing alloy (see Figures 8 and 12).

4. Conclusions

The microstructural behavior after dilution of a Fe-based hardfacing alloy containing a high amount of carbide-boride forming elements was studied. The addition of up to 50 mass % Fe shifted the microstructure from an almost fully hypereutectic structure to a hypoeutectic structure. The effect of dilution on the solidification behavior was remarkable, particularly when the eutectic composition was obtained. In this condition the solidification range reached a minimum value. The hardness and wear properties of the diluted alloys were greatly influenced when the dilution level became higher than 30 mass % Fe. The analyzed effects of the dilution are considered to be of significant importance for the optimization of cladding alloy properties along the full thickness of the coatings.

Conflict of Interests

The authors declare that there is no conflict of interests regarding the publication of this paper.

Acknowledgment

The present research was financed under the research project DEBACOAT (development of high-performance barrels with innovative gradient coatings) funded by the European Commission under the call FP7-SME-2012 (Project ID: 315417).

References

[1] E. O. Correa, N. G. Alcântara, D. G. Tecco, and R. V. Kumar, "The relationship between the microstructure and abrasive resistance of a hardfacing alloy in the Fe-Cr-C-Nb-V system," *Metallurgical and Materials Transactions A*, vol. 38, no. 8, pp. 1671–1680, 2007.

[2] H. Berns, "Comparison of wear resistant MMC and white cast iron," *Wear*, vol. 254, no. 1-2, pp. 47–54, 2003.

[3] R. J. Chung, X. Tang, D. Y. Li, B. Hinckley, and K. Dolman, "Microstructure refinement of hypereutectic high Cr cast irons using hard carbide-forming elements for improved wear resistance," *Wear*, vol. 301, no. 1-2, pp. 695–706, 2013.

[4] T. T. Matsuo, C. S. Kiminami, W. J. B. Fo, and C. Bolfarini, "Sliding wear of spray-formed high-chromium white cast iron alloys," *Wear*, vol. 259, no. 1–6, pp. 445–452, 2005.

[5] S. Lee, S.-H. Choo, E.-R. Baek, S. Ahn, and N. J. Kim, "Correlation of microstructure and fracture toughness in high-chromium white iron hardfacing alloys," *Metallurgical and Materials Transactions A: Physical Metallurgy and Materials Science*, vol. 27, no. 12, pp. 3881–3891, 1996.

[6] L. St-Georges, "Development and characterization of composite Ni-Cr + WC laser cladding," *Wear*, vol. 263, no. 1–6, pp. 562–566, 2007.

[7] B. Valsecchi, B. Previtali, and E. Gariboldi, "Fibre laser cladding of turbine blade leading edges: the effect of specific energy on clad dilution," *International Journal of Structural Integrity*, vol. 3, no. 4, pp. 377–395, 2012.

[8] T. Lucey, R. Wuhrer, K. Moran, M. Reid, P. Huggett, and M. Cortie, "Interfacial reactions in white iron/steel composites," *Journal of Materials Processing Technology*, vol. 212, no. 11, pp. 2349–2357, 2012.

[9] I. Hemmati, V. Ocelík, and J. T. M. De Hosson, "Effects of the alloy composition on phase constitution and properties of laser deposited Ni-Cr-B-Si coatings," *Physics Procedia*, vol. 41, pp. 302–311, 2013.

[10] J. Campbell, *Castings*, Butterworth Heinemann, Oxford, UK, 2nd edition, 2003.

[11] C.-M. Chang, C.-M. Lin, C.-C. Hsieh, J.-H. Chen, and W. Wu, "Micro-structural characteristics of Fe-40 wt%Cr-*x*C hardfacing alloys with [1.0–4.0 wt%] carbon content," *Journal of Alloys and Compounds*, vol. 487, no. 1-2, pp. 83–89, 2009.

[12] I. Hemmati, V. Ocelík, and J. T. M. de Hosson, "Dilution effects in laser cladding of Ni-Cr-B-Si-C hardfacing alloys," *Materials Letters*, vol. 84, pp. 69–72, 2012.

[13] A. Röttger, S. Weber, and W. Theisen, "Supersolidus liquid-phase sintering of ultrahigh-boron high-carbon steels for wear-protection applications," *Materials Science and Engineering A*, vol. 532, pp. 511–521, 2012.